4

Two-Fluxes and Reaction-Diffusion Computation of Initial and Transient Secondary Electron Emission Yield by a Finite Volume Method

Asdin Aoufi[1] and Gilles Damamme[2]
[1]*SMS/RMT, PECM, UMR CNRS 5146, Ecole des Mines de Saint-Etienne, 158 cours Fauriel, 42023 Saint-Etienne Cedex*
[2]*CEA -DAM/DIF, 91680 Bruyères le Châtel France*

1. Introduction

Dielectric breakdown in insulating materials is related to fast relaxation of trapped charges according to (G. Damamme & Reggi, 1997) and is of practical importance since it damages electronic devices (Levy, 2002). In fact, it is known that the secondary electron emission yield (*denoted by see*) is one of the key parameters for dielectric materials. Moreover, *see* is the driving parameter of electric charging which can lead to electric breakdown. To study this phenomena, the behaviour of an insulator submitted to an electron beam irradiation is considered. This has led to a significant number of experimental studies since the discovery of this phenomena. Although several modelling such as in (I.A.Glavatskikh & Fitting, 2001),(Fitting, 1974) and (H.-J. Fitting & Wild, 1977) are available in literature, they do not provide a simple method to compute the initial *see* yield from the penetration depth of the incident electron beam, and some material characteristics. The purpose of the work detailed in the book chapter is to describe such a simple modelling related to electron/matter interaction for low values of incident electron beam's energy and the tight coupling between modelling, numerical analysis and comparison with some experimental results.
This book chapter presents in a unified manner, published and new results. We focuss the presentation on our numerical/software approach, and comparison with experimental results.
In section 2, we propose a new modelling for the initial see yield computation. The main contribution is that we have reanalyzed from a mathematical point of view the modelling, stating that there exists a unique solution, which is uniformly bounded and which fulfill a maximum principle. From a numerical point of view, we have used a classical upwind finite-volume scheme, and shown the existence, uniqueness and discrete maximum principle for the discrete numerical solution. Finally a new asymptotic expression for the expression of see yield for large values of the electron beam energy is presented and discussed.
In section 3, we show that the computation of the initial see yield by a two-fluxes method, which requires the solution of a set of two coupled differential equations described in section 2, can in fact be reformulated into a single reaction-diffusion problem, which is much easier to solve from a computational point of view, since a single tri-diagonal matrix has to be inverted.

This appears to be a new result in this field.
In section 4, we present a model which computes the evolution of transient secondary electron emission yield. It is based upon a set of conservation laws which expresses the trapping of electrons and holes coupled with the electric field. From a numerical point of view, we apply a fully implicit scheme and uses a simple, fixed point technique to the solves the coupled set of discrete equations, and use a refined grid near the interface where the electron beam penetrates the sample. This enhances the quality of the numerical simulation and reduces significantly the elapsed computational time compared to Fitting's works (I.A.Glavatskikh & Fitting, 2001),(Fitting, 1974) and (H.-J. Fitting & Wild, 1977)¿Q, which is constrained by the fixed mesh spacing used in the presentation of his modelling. Moreover our numerical scheme uses the conservative finite-volume method, and we have proved formally that some discrete maximum principle occur which provides confidence in our numerical work. Some comparison between numerical computations and experimental work by G. Moya (IM2MP, Marseille, France) and K. Zarbout (IM2MP, Marseille, France, and LamaCop, Sfax, Tunisia) are presented.
In section 5, we extend the reformulation of the two-fluxes modelling presented in section 4 into a reaction-diffusion modelling. The main strength of this new approach is the ability to be extended easily in two spatial dimensions, while it is more difficult to extend in two-spatial dimensions the two-fluxes approach borrowed from the radiative transfer (**?**), hence this new approach seems more promising.
In section 6, we present the main architecture of our numerical software **sirena**.
We conclude this chapter with section 7, which summarizes the obtained results and draws some perspective of future work.

2. Initial see computation by a two-fluxes method

This section presents a modelling describing the generation of secondary electrons. The slowdown of primary electrons creates free electrons/holes pairs. A diffusion movement of these particles occurs. Some of the secondary electrons generated near the surface could be emitted when they are not trapped before.

2.1 Mathematical modelling

Let $C = \{e+,e-\}$, the charge transport of current fluxes $(j_c(z))_{c\in C}$ is described by a one-dimensional system of coupled linear differential equations along the z-axis. A two-fluxes method derived from radiative transfert theory is used which splits the electron current $j_e(z)$ into forward $j_{e+}(z)$ and backward $j_{e-}(z)$ contributions such that the algebraic currents verify $j_e(z) = j_{e+}(z) - j_{e-}(z)$. The coupling between $j_{e+}(z)$ and $j_{e-}(z)$ fluxes is written and takes into account diffusion.

$$-\frac{dj_{e-}(z)}{dz} + \left(\sigma_{e-}^{diff} + \sigma_e^{abs}\right) j_{e-}(z) = S_e(z) + \sigma_{e+}^{diff}\, j_{e+}(z), \tag{1}$$

with boundary condition $j_{e-}(L) = 0$, and

$$\frac{dj_{e+}(z)}{dz} + \left(\sigma_{e+}^{diff} + \sigma_e^{abs}\right) j_{e+}(z) = S_e(z) + \sigma_{e-}^{diff}\, j_{e-}(z). \tag{2}$$

with boundary condition $j_{e+}(0) = (1-\kappa)\ j_{e-}(0)$, where $\kappa \in [0,1]$ is the transmission coefficient, σ_e^{abs},$\sigma_{e\pm}^{diff}$ are respectively absorption and diffusion cross sections. This

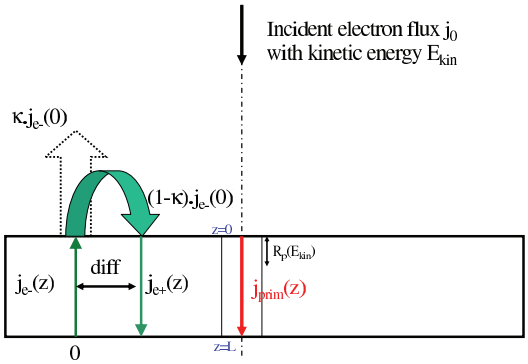

Fig. 1. Scheme of the modelling assuming that there is no backscattered electrons and where R_p is the penetration thickness and L is the dielectric thickness. The incident electron flux j_0 has a kinetic energy E_{kin}.

mathematical modelling is used to analyse the sensibility of the true secondary electron emission yield see^* defined by the expression

$$see^* = \kappa \frac{j_{e-}(0)}{j_0}. \tag{3}$$

with respect to the relative importance of charges absorption/diffusion inside the material, where j_0 is the current density of primary electrons (the backscattered electrons being excluded) and κ is the transmission coefficient.

2.2 Existence-uniqueness of the formal solution

The following proposition was presented in (Aoufi & Damamme, 2009)

Proposition 2.1 *Denoting the constant* $\sigma_c = \sigma_e^{abs} + \sigma_c^{diff}$, *and under the assumption that* $[z \mapsto S_e(z)]$ *is continuous over* Ω, *then*

– *the problem has a unique solution* $(j_{e-}(z), j_{e+}(z))$ *for* $z \in \Omega$ *given by the coupled system*

$$j_{e-}(z) = \int_z^L \left(S_e(E_{kin}, u; j_0) + \sigma_{e+}^{diff} j_{e+}(u) \right) e^{\sigma_{e-}(z-u)} du. \tag{4}$$

$$j_{e+}(z) = j_{e+}(0).e^{-\sigma_{e+}z} + \int_0^z \left(S_e(E_{kin}, u; j_0) + \sigma_{e-}^{diff} j_{e-}(u) \right) e^{\sigma_{e+}(u-z)} du. \tag{5}$$

– *Moreover there exits a constant* $C\left(\|S_e\|_{L^\infty(\Omega)}, E_{kin}, L, \sigma_e^{abs}, \sigma_c^{diff} \right) > 0$ *such that for* $z \in \Omega$

$$0 \le j_{e-,+}(z) \le j_0.C\left(\|S_e\|_{L^\infty(\Omega)}, E_{kin}, j_0, L, \sigma_e^{abs}, \sigma_c^{diff} \right)$$

2.3 Asymptotic expression for the secondary electron emission yield

Proposition 2.2 *We define the transfer cross section* $\sigma_e^{trans} = \sigma_e^{abs} + \sigma_{e+}^{diff} + \sigma_{e-}^{diff}$, *Under the asymption that* $1 \ll \sigma_e^{abs}.R_p(E_{kin})$ *then*

$$see^* \simeq \kappa \frac{S_e(z=0, E_{kin})}{\sigma_e^{abs}} \frac{\sigma^*}{\sigma_e^{trans}} \frac{\sigma^*}{(1-\frac{\kappa}{2})\sigma_e^{abs} + \frac{\kappa}{2}\sigma^*}. \tag{6}$$

where

$$\Delta\sigma_e^{diff} = \sigma_{e+}^{diff} - \sigma_{e-}^{diff},\ 2\sigma^* = \Delta\sigma_e^{diff} + \sqrt{\left(4\sigma_e^{abs}\,\sigma_e^{trans} + \left(\Delta\sigma_e^{diff}\right)^2\right)}. \tag{7}$$

Fig.(2) represents a comparison between asymptotic formula given by Eq.(6) and computation of *see* yield from Eq.(3). A good agreement is observed for high values of E_{kin}. Other computational results are given in (Aoufi & Damamme, n.d.).

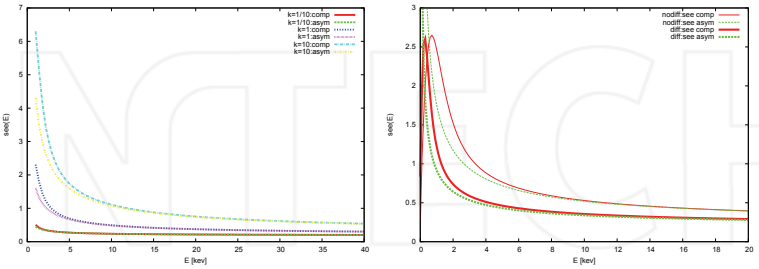

Fig. 2. (a) Comparison between computed and asymptotic expression for see yield in the case where $\sigma_{e+}^{diff} = k\sigma_e^{diff}$ and $\sigma_{e-}^{diff} = k^{-1}\sigma_e^{diff}$ with $k \in \{1/10, 1, 10\}$. (b) Comparison between numerical values and asymptotic expression of $see^*\left(E_{kin}\right)$ as a function of E_{kin} [kev] in both cases with and without diffusion (for $\sigma_c^{diff} = \sigma_{\overline{c}}^{diff}$).

2.4 Numerical scheme

A vertex-centered conservative finite-volume discretization of the governing equation with an adequate upwind technique is defined. The domain Ω is decomposed into a set of I control volumes $\Omega_i = [z_i, z_{i+1}]$ with length $h_{i+\frac{1}{2}}$. The discrete unknown at grid point z_i related to j_c is denoted $j_c|_i$.

Proposition 2.3 *Denoting* $S_{i+\frac{1}{2}} = S_e\left(z_{i+\frac{1}{2}}\right)$, *where* $z_{i+\frac{1}{2}} = \frac{1}{2}\left(z_i + z_{i+1}\right)$, *then*

– *the scheme obtained after integrating the forward linear equation over* $\Omega_{i+\frac{1}{2}}$ *is written for each cell index* i,

$$\begin{aligned} &\frac{j_{e+}|_{i+1} - j_{e+}|_i}{h_{i+\frac{1}{2}}} + \left(\sigma_e^{abs} + \sigma_{e+}^{diff} + \sigma_{e-}^{diff}\right).\, j_{e+}|_{i+1} \\ = \;& S_{i+\frac{1}{2}} + \sigma_{e-}^{diff}\left(j_{e-}|_{i+1} + j_{e+}|_i\right) \end{aligned} \tag{8}$$

– *using a similar computation, the scheme for the backward linear equation leads to the discrete equation*

$$\begin{aligned} &-\frac{j_{e-}|_i - j_{e-}|_{i-1}}{h_{i-\frac{1}{2}}} + \left(\sigma_e^{abs} + \sigma_{e+}^{diff} + \sigma_{e-}^{diff}\right).\, j_{e-}|_{i-1} \\ = \;& S_{i-\frac{1}{2}} + \sigma_{e+}^{diff}\left(j_{e+}|_{i-1} + j_{e-}|_i\right). \end{aligned} \tag{9}$$

– *The linear system with the discrete unknowns* $\left(j_{e-}|_i\right)_{1\le i\le I+1}, \left(j_{e+}|_i\right)_{1\le i\le I+1}$ *has a unique solution,*

– *which verify a discrete maximum principle for a suitable constant* $C > 0$

$$0 \leq j_{e-,+}|_i \leq C \tag{10}$$

2.5 Numerical simulations

Fig.(3) shows that in a suitable normalized representation, the evolution of secondary electron emission yield has a similar shape for different expressions of the penetration depth radius.

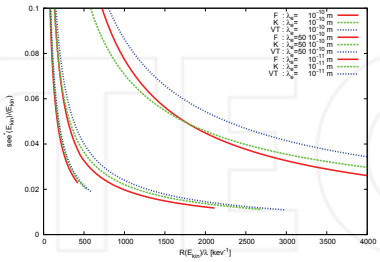

Fig. 3. Reduced variables evolution of $\frac{see^*(E_{kin})}{E_{kin}}$ in eV^{-1} as a function of $\frac{R(E_{kin})}{\lambda_e^{abs}}$ for the three penetration radius $R_p(E)$ laws, Vyatskin and Trunev (VT), Kanaya (K) and Fitting (F) for differents values of λ_e^{abs}.

3. Initial see computation by a reaction-diffusion method

3.1 Mathematical modelling

In order to reformulate Eq.(1)-(2) into a reaction diffusion equation, let us define the number of free electrons per unit volume $n_e(z)$ such that for $z \in [0, L]$, $v_e n_e(z) = j_{e+}(z) + j_{e-}(z)$ with v_e the mean absolute velocity of charge carriers and the overall transfert cross-section σ_e^{trans} according to $\sigma_e^{trans} = \sigma_e^{abs} + 2\sigma_e^{diff}$. After summation and substraction of Eq(1)-(2), and using the definition of $j_e(z)$ and $n_e(z)$ one obtain that

$$\frac{dj_e(z)}{dz} = 2S_e(z) - <\sigma_e^{abs} v_e> n_e(z),\ v_e \frac{dn_e(z)}{dz} = -j_e(z)\ \sigma_e^{trans}. \tag{11}$$

Defining the diffusion coefficient $D_e = \frac{v_e}{\sigma_e^{trans}}$ with respect to the transfer equation leads to the fact that the current flux $j_e(z)$ follows a Fick-type law : $j_e(z) = -D_e \frac{dn_e(z)}{dz}$. Pluging this expression into Eq.(3) leads to the reaction-diffusion equation with Fourier type boundary conditions

$$-D_e \frac{d^2 n_e(z)}{dz^2} = 2S_e(z) - <\sigma_e^{abs} v_e> n_e(z) \tag{12}$$

$$D_e \frac{dn_e(0)}{dz} = \frac{\kappa}{2-\kappa} n_e(0) v_e, \tag{13}$$

$$D_e \frac{dn_e}{dz}(L) = -n_e(L) v_e \tag{14}$$

The reformulation of Eq.(3) in terms of the number of trapped electrons $n_e(z)$ is easily obtained thanks to Eq.(11) and is such that :

$$see^* = \frac{\kappa}{2-\kappa}\frac{n_e(0)\,v_e}{j_0} \tag{15}$$

It is worth mentioning that in the case of electron transport, the velocity v_e can be obtained thanks to the equation $\frac{1}{2}m_e v_e^2 = E_e$ where the energy E_e was between $1\text{eV} - 3\text{eV}$, and is related to value of the gap energy.

3.2 Numerical scheme

A cell-centered finite-volume scheme on a geometrically refined grid near interface $z = 0$ is used. We prove the existence and uniqueness of the discrete solution that is computed by the inversion of a sparse tridiagonal matrix thanks to the classical Thomas algorithm -i.e. Gauss method for tridiagonal matrices-. We prove a discrete maximum principle, thanks to the M-matrix property of the tri-diagonal matrix.
We use a classical cell-centered finite volume approximation on computational domain Ω. A set of non-uniformly spaced grid points $(z_i)_{1\le i\le i+1}$ is given, and is such that $z_1 = 0 < \cdots < z_i < \ldots z_{I+1} = L$. We denote by h_i the length of control volume $\Omega_i = [z_i, z_{i+1}]$ and n_i the mean of $n(z)$ over control volume Ω_i. There are $I+1$ nodes, but I control volumes.

Proposition 3.1 *The finite-volume discretization of Eq.(14) leads to the following linear system*

$$\begin{pmatrix} b_1 & c_1 & & & \\ & \ddots & & & \\ & a_i & b_i & c_i & \\ & & & \ddots & \\ & & & a_I & b_I \end{pmatrix} \begin{pmatrix} n_1 \\ \vdots \\ n_i \\ \vdots \\ n_I \end{pmatrix} = \begin{pmatrix} 2h_1 S_1 \\ \vdots \\ 2h_i S_i \\ \vdots \\ 2h_I S_I \end{pmatrix}$$

with

$$a_1 = 0, \quad b_1 = \frac{D_e}{h_1 + \frac{h_2}{2}} + \frac{\kappa}{2-\kappa}v_e + < \sigma_e^{abs} v_e > h_1, \quad c_1 = -\frac{D_e}{h_1 + \frac{h_2}{2}}, \tag{16}$$

and for $i \in [1, I-1]$

$$a_i = \frac{D_e}{\frac{h_i + h_{i-1}}{2}}, \quad b_i = -\frac{D_e}{\frac{h_i + h_{i+1}}{2}} + \frac{D_e}{\frac{h_i + h_{i-1}}{2}} + < \sigma_e^{abs} v_e > h_i, \quad c_i = -\frac{D_e}{\frac{h_i + h_{i+1}}{2}}, \tag{17}$$

and

$$a_I = 0, \quad b_I = -\frac{D_e}{h_I + \frac{h_{I-1}}{2}}, \quad c_I = \frac{D_e}{h_I + \frac{h_{I-1}}{2}} + v_e. \tag{18}$$

which has a unique **positive solution.**

The discretization of Eq.(14) over control volume Ω_i leads to the following discrete equation which is specialized if $i = 1$, or $1 < i < I$ or $i = I$

$$-D_e\frac{n_2-n_1}{h_1+\frac{h}{2}}+\frac{\kappa}{2-\kappa}n_1 v_e = 2h_1 S_1 + < \sigma_e^{abs} v_e > n_1 h_1 \quad (19)$$

$$-D_e\frac{n_{i+1}-n_i}{\frac{h_i+h_{i+1}}{2}}+D_e\frac{n_i-n_{i-1}}{\frac{h_i+h_{i-1}}{2}} = 2h_i S_i + < \sigma_e^{abs} v_e > n_i h_i \quad (20)$$

$$v_e n_I + D_e\frac{n_I-n_{I-1}}{h_I+\frac{h_{I-1}}{2}} = 2h_I S_I + < \sigma_e^{abs} v_e > n_I h_I \quad (21)$$

The matrix of the linear system that is used to compute $(n_i)_{1\leq i\leq I+1}$ is an M-matrix, since

- $b_i \geq 0,\ a_i, c_i \leq 0,\ b_i \geq |a_i| + |c_i|$,
- and $2h_i S_i \geq 0$.

we conclude that it is invertible and that the unique solution of the linear system is positive.

3.3 Numerical simulations

The evolution of $n_e(z)$ is depicted in Fig.(4). It is seen that $n_e(z) \geq 0$, and that its shape is closely influenced by the expression used for $S_e(z)$.

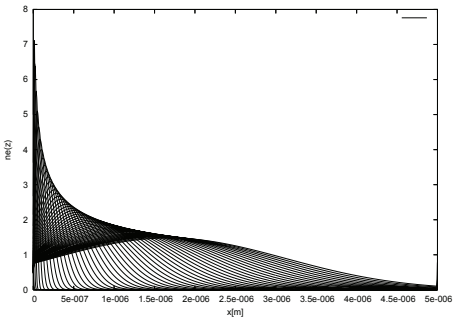

Fig. 4. Spatial distribution of $n_e(z)$ for various values E_{kin}.

4. Transient see computation by a two-fluxes method

In section 4, the modelling borrows from Fitting's papers, the absorption/diffusion cross-section expressions as a function of electric field. It differs mainly in the governing set of equations and in the numerical techniques that are used but also in the fact that some comparison between numerical computations and experimental work are done.

4.1 Mathematical modelling

The mathematical modelling expresses the coupling between electric field with electron/hole transport and describes the spatial and temporal charge trapping in an insulator submitted to an electron beam irradiation. The temporal evolution of the secondary electron emission is computed as a function of global trapped charge. It is given by a set of 7 nonlinear, coupled equations.

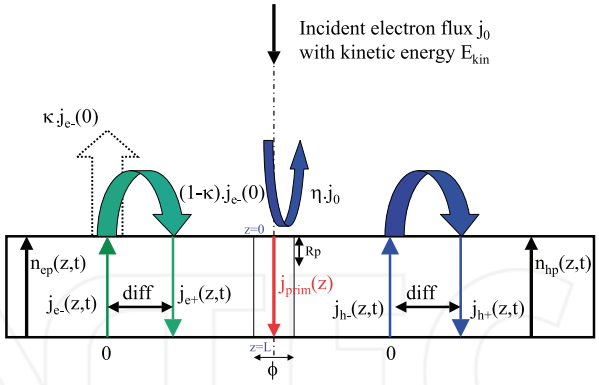

Fig. 5. Scheme of the modelling where R_p is the penetration depth, ϕ the diameter of the irradiated zone and L the dielectric thickness. The incident electron flux j_0 has a kinetic energy E_{kin}. Scheme of the modelling where $R_p(E_{kin})$ is the penetration depth, ϕ the diameter of the irradiated zone and L the dielectric thickness. The incident electron flux j_0 has a kinetic energy E_{kin}. The electron fluxes j_{e-}/j_{e+} and the hole fluxes j_{h-}/j_{h+} are coupled by diffusion.

4.1.1 Purpose of the modelling

The purpose of this modelling is to analyze the evolution of the global trapped charge, per unit surface, at time t, $Q_p(t)$ which is defined by:

$$Q_p(t) = \int_0^L \rho(z,t)\,dz + |e|\,n_s(t) \tag{22}$$

and the true secondary electron emission yield $see^*(t)$ expressed as:

$$see^*(t) = \kappa_s\left(n_s(t)\right)\frac{j_{e-}(0,t)}{j_0} \tag{23}$$

where the expression of $\kappa\left(n_s(t)\right)$ is given in the next subsubsection.
The proposed modelling describes the interaction between the number of trapped electrons $n_{ep}(z,t)$ and holes $n_{hp}(z,t)$ with the four current fluxes $(j_c)_{c\in\mathcal{C}}$, the current $j_{prim}(z)$ and the electric field $E(z,t)$.

4.1.2 Governing equation for the saturation effect of the surface trapping sites $n_s(t)$

Defining by N_s the number of trapping surface sites located at the interface $z = 0$ and by σ_s their elementary cross section then the evolution of the number of traps per surface unit at time t, $n_s(t)$ follows the equation

$$|e|\,\frac{dn_s(t)}{dt} = j_{e-}(0,t)\left(\kappa - \kappa_s\left(n_s(t)\right)\right) \tag{24}$$

where $\kappa_s\left(ns(t)\right)$ is defined by:

$$\kappa(n_s(t)) = \kappa\exp\left(-\sigma_s\left(N_s - n_s(t)\right)\right) \tag{25}$$

Its contribution is especially important during the initial charge injection phase for an amount of time driven by the product $\sigma_s N_s$. The initial condition states that there are no surface trapped charges.

4.1.3 Governing equation for the electric field $\mathbf{E}(\mathbf{z},\mathbf{t})$

Here we assume that the electric field $E(z,t)$ depends only on the total charge density $\rho(z,t)$ which is different from the trapped charge density. Using a two-fluxes method it was assumed that only the trapped charge density contributed to the electric field. The local Maxwell-Gauss equation writes

$$\nabla.E\left(z,t\right)=\frac{\rho\left(z,t\right)}{\epsilon_0\epsilon_r}, \tag{26}$$

An electrostatic analysis taking into account polarization charges on the interface leads to

$$E\left(0,t\right)=-\frac{1}{\epsilon_0\epsilon_r\left(1+\varepsilon_r\right)}\,\frac{1}{1+\frac{\pi\phi^2/4}{L^2(1+\varepsilon_r)}}\,Q_p(t)-|e|\frac{n_s(t)}{\epsilon_0\epsilon_r}. \tag{27}$$

where the second factor is introduced as corrections due to image charges in the sample holder.

4.1.4 Governing equation for current fluxes $j_c\left(z,t\right)$

The following balance is written

$$d_c\frac{\partial j_c(z,t)}{\partial z}+\sum_{i=1}^{3}W_{c,i}=S_c(z)+\sigma_c^{diff}\left(E(z,t)\right)j_c(z,t) \tag{28}$$

where

(a) $d_c\frac{\partial j_c(z,t)}{\partial z}$ is the gradient of forward/backward electron/hole flux,

(b) $W_{c,1}=\sigma_c^{diff}\left(E(z,t)\right)j_c(z,t)$ is the flux loss by diffusion,

(c) $W_{c,2}=\left(\sigma_{pc}\left(N_{pc}-n_{cp}(z,t)\right)\right).j_c(z,t)$, is the flux loss by trapping on unoccupied trapping sites $N_{pc}-n_{cp}(z,t)$,

(d) $W_{c,2}=\sigma_{ac}n_{\hat{c}p}(z,t)j_c(z,t)$ is the flux loss by annihilation with trapped charge $\hat{c}$,

(e) $S_c(z)$ is a source term for the creation of electrons or holes induced by the slowdown of primary electrons.

(f) $\sigma_c^{diff}\left(E(z,t)\right)j_c(z,t)$ is a positive source transport term by diffusion for dual charge of c, i.e. travelling in the opposite direction.

The boundary conditions are s_c sign dependant.

- For backward fluxes $j_{e-}\left(z,t\right)$ and $j_{h-}\left(z,t\right)$, the boundary condition at $z=L$ means that the bottom of the material has no charge injection: $\forall c\in\{e-,h-\}\ :\ j_c\left(L,t\right)=0$.
- For forward fluxes, $j_{e+}\left(z,t\right)$ and $j_{h+}\left(z,t\right)$, the boundary condition at $z=0$ means the continuity of the hole flux $j_{h+}\left(0,t\right)=j_{h-}\left(0,t\right)$, but a discontinuity for the electron flux $j_{e+}\left(0,t\right)=\left(1-\kappa\right).j_{e-}\left(0,t\right)$.

4.1.5 Governing equation for the charge density $\rho\left(z,t\right)$

The temporal variation of the trapped charge density $\rho(z,t)$ follows the conservation law

$$\frac{\partial\rho\left(z,t\right)}{\partial t}+\nabla.j\left(z,t\right)=0, \tag{29}$$

where the overall current flux of charges $j\left(z,t\right)$ is such that

$$j\left(z,t\right)\quad=\quad j_{e-}\left(z,t\right)-j_{e+}\left(z,t\right)-j_{h-}\left(z,t\right)+j_{h+}\left(z,t\right)-j_0\,j_{prim}\left(z\right). \tag{30}$$

4.1.6 Governing equation for trapped charge $Q_p(t)$

The temporal evolution of total trapped charge $Q_p(t)$ is defined from the total charge density

$$\rho(z,t) = |e| \left(n_{ep}(z,t) - n_{hp}(z,t) \right) \tag{31}$$

thanks to the equation

$$\frac{dQ_p(t)}{dt} = \int_0^L \frac{d\rho(z,t)}{dt} = -j_{e+}(L,t) + j_{h+}(L,t) + j_0(1 - see(t)). \tag{32}$$

4.1.7 Governing equation for the trapped electrons $n_{ep}(z,t)$

The evolution of the number of trapped electrons $n_{ep}(z,t)$ follows the differential equation

$$\begin{aligned} |e| \frac{\partial n_{ep}}{\partial t}(z,t) &= \sigma_{pe} \left(N_{pe} - n_{ep}(z,t) \right) \left(j_{e+}(z,t) + j_{e-}(z,t) \right) \\ &\quad - \sigma_{ah} n_{ep}(z,t) \left(j_{h+}(z,t) + j_{h-}(z,t) \right) \end{aligned} \tag{33}$$

which expresses the balance between

– the number of electrons that are trapped, where σ_{pe} is the trapping cross section of the electrons and N_{pe} is the total number of electrons trapping sites,

$$\sigma_{pe} \left(N_{pe} - n_{ep}(z,t) \right) \left(j_{e+}(z,t) + j_{e-}(z,t) \right) \tag{34}$$

– and the number of trapped electrons present in the traps that are annihilated by free holes, where σ_{ah} is the annihilation cross section between trapped electrons and free holes.

$$\sigma_{ah} n_{ep}(z,t) \left(j_{h+}(z,t) + j_{h-}(z,t) \right). \tag{35}$$

The absolute value, $|e|$ of the electron charge in coulomb is introduced to transform the fluxes $(j_c(z,t))_{c \in C}$ expressed in Coulomb into fluxes expressed in carriers numbers.
The initial condition $n_{ep}(z,0) = 0$, means that there are no trapped electrons at the beginning of charge injection.

Remark 4.1 *In order to simplify the notations, we define the total flux* $j^T_{h,e}(z,t) = j_{h+/e+}(z,t) + j_{h-/e-}(z,t)$, *which is always positive, while the algebraic flux* $j_{h,e}(z,t) = j_{h+/e+}(z,t) - j_{h-/e-}(z,t)$ *can be negative. We introduce functions* $a(z,t)$ *and* $b(z,t)$ *that are defined by the expressions*

$$\begin{aligned} a(z,t) &= \left(\sigma_{pe} j^T_e(z,t) + \sigma_{ah} j^T_h(z,t) \right) / |e| \geq 0, \\ b(z,t) &= \left(\sigma_{pe} N_{pe} j^T_e(z,t) \right) / |e| \geq 0. \end{aligned}$$

then Eq.(33) can be rewritten

$$\frac{\partial n_{ep}}{\partial t}(z,t) + a(z,t) n_{ep}(z,t) = b(z,t) \tag{36}$$

A straightforward computation shows that the formal solution of Eq.(33) is given by

$$n_{ep}(z,t) = \int_0^t \exp^{\int_t^v a(z,u)\,du} b(z,v)\,dv \tag{37}$$

from which we can infer that $n_{ep}(z,t) \geq 0$.

4.1.8 Governing equation for the trapped holes $n_{hp}(z,t)$

The evolution of the number of trapped holes $n_{hp}(z,t)$ follows the differential equation

$$\begin{aligned} |e|\frac{\partial n_{hp}}{\partial t}(z,t) &= \sigma_{ph}\left(N_{ph}-n_{hp}(z,t)\right)\left(j_{h+}(z,t)+j_{h-}(z,t)\right) \\ &\quad -\sigma_{ae}n_{hp}(z,t)\left(j_{e+}(z,t)+j_{e-}(z,t)\right) \end{aligned} \tag{38}$$

which expresses the balance between

- the number of holes that are trapped, where σ_{ph} is the trapping cross section of the holes and N_{ph} is the total number of holes trapping sites,

$$\sigma_{ph}\left(N_{ph}-n_{hp}(z,t)\right)\left(j_{h+}(z,t)+j_{h-}(z,t)\right) \tag{39}$$

- and the number of trapped holes present in the traps that are annihilated by free electrons, where σ_{ae} is the annihilation cross section between trapped holes and free electrons.

$$\sigma_{ae}n_{hp}(z,t)\left(j_{e+}(z,t)+j_{e-}(z,t)\right) \tag{40}$$

The initial condition $n_{hp}(z,0)=0$, means that there are no trapped holes at the beginning of charge injection.
It is worth mentioning that trapped holes and trapped electrons have the same type of behaviour, so the governing equations are symmetrical, when one exchanges the index h with the index e.

4.2 Numerical scheme

The mathematical modelling expresses the nonlinear coupling between a set of seven equations with seven unknowns $E(z,t)$, $(j_c(z,t))_{c\in\mathcal{C}}$, $n_{ep}(z,t)$ and $n_{hp}(z,t)$. A straighforward computation leads to a formal expression of each unknown as a function of the others which involves spatial/temporal integrals and stiff exponential functions, but the non-linear coupling remain. We are therefore led to use a numerical discretization scheme to compute the solution of this one-dimensional nonlinear initial boundary value problem, expressed in conservation form.
We present a full implicit conservative finite volume scheme on a non uniform **staggered grid** used for the discretization of the governing set of equations on a geometrically refined grid near the interface z=0. The computational domain is Ω.

- Unknowns that are located at the **center of cell** Ω_i are $n_{ep}|_i^k$, $n_{hp}\Big|_i^k$, $\rho|_i^k$,
- Unknowns that are located at the **edges of cell** Ω_i **are** $E|_{i,i+1}^k$, $j_{e+}|_{i,i+1}^k$, $j_{e-}|_{i,i+1}^k$, $j_{h+}|_{i,i+1}^k$, $j_{h-}|_{i,i+1}^k$.

We use a backward Euler scheme, with constant time-step Δt, first order accurate in time, for the temporal discretization, and note $t_k = k.\Delta t$.

4.2.1 Discretization of the surface trapping sites $n_s(t)$ equation

A straightforward computation leads to the discrete equation

$$\frac{n_s^{k+1}-n_s^k}{\Delta t}=\frac{j_{e-}|_1^{k+1}}{|e|}\left(\kappa-\kappa_s(n_s^{k+1})\right). \tag{41}$$

The stiffness induced by the exponential term present in $\kappa_s(n_s^{k+1})$ requires a first order linearization, hence the iterative solution by a fixed point technique is given by

$$\frac{n_s^{k+1,p+1} - n_s^{k,p}}{\Delta t} = \frac{j_{e-}|_1^{k+1,p}}{|e|}(\kappa - w^p)), \tag{42}$$

$$w^p = \kappa_s(n_s^{k+1,p}) + \left(n_s^{k+1,p+1} - n_s^{k+1,p}\right)\kappa_s'(n_s^{k+1,p}). \tag{43}$$

Then the value of $n_s^{k+1,p+1}$ is easily determined.

4.2.2 Discretization of the charge density equation

Integrating Eq.(29) over control volume Ω_i leads to the discrete equation

$$h_i\left(\rho_i^{k+1} - \rho_i^k\right) + \Delta t\left(j_{i+1}^{k+1} - j_i^{k+1}\right) = 0. \tag{44}$$

A decoupled iterative solution thanks to the fixed point method leads to the computation, where p is the nonlinear iteration index

$$\rho_i^{k+1,p+1} = \rho_i^k - \frac{\Delta t}{h_i}\left(j_{i+1}^{k+1,p} - j_i^{k+1,p}\right). \tag{45}$$

4.2.3 Discretization of the trapped charge equation

The discretization is straightforward and leads to the equation

$$\frac{Q_p|^{k+1} - Q_p|^k}{\Delta t} = -j_{e+}|_{I+1}^{k+1} + j_{h+}|_{I+1}^{k+1} + j_0\left(1 - see^{k+1}\right). \tag{46}$$

A decoupled iterative solution thanks to the fixed point method leads to the computation, where p is the nonlinear iteration index

$$Q_p|^{k+1,p+1} = Q_p|^{k,p} + \Delta t\left(-j_{e+}|_{I+1}^{k+1,p} + j_{h+}|_{I+1}^{k+1,p} + j_0\left(1 - see^{k+1,p}\right)\right). \tag{47}$$

4.2.4 Discretization of the electric field equation

The discretization is straightforward and leads to the equation

$$E_{i+1}^{k+1} - E_i^{k+1} = \frac{h_i\rho_i^{k+1}}{\epsilon_0\epsilon_r}, \tag{48}$$

$$E_1^{k+1} = -\frac{1}{\epsilon_0\epsilon_r\left(1+\varepsilon_r\right)}\frac{1}{1+\frac{\pi\phi^2/4}{L^2(1+\varepsilon_r)}}Q_p^{k+1} - |e|\frac{n_s^{k+1}}{\epsilon_0\epsilon_r}. \tag{49}$$

A decoupled iterative solution thanks to the fixed point method leads to the computation, where p is the nonlinear iteration index.

$$E_{i+1}^{k+1,p+1} = E_i^{k+1} + \frac{h_i\rho_i^{k+1,p}}{\epsilon_0\epsilon_r}, \tag{50}$$

$$E_1^{k+1,p+1} = -\frac{1}{\epsilon_0\epsilon_r\left(1+\varepsilon_r\right)}\frac{1}{1+\frac{\pi\phi^2/4}{L^2(1+\varepsilon_r)}}Q_p^{k+1,p} - |e|\frac{n_s^{k+1,p}}{\epsilon_0\epsilon_r}. \tag{51}$$

4.2.5 Discretization of the trapped holes's number equation

In order to simplify the notations all the cross section terms are divided by the factor $|e|$.

Proposition 4.1 *The finite volume discretization of Eq.(38) over control volume Ω_i leads to the discrete equation*

$$\frac{n_{hp}\Big|_i^{k+1} - n_{hp}\Big|_i^{k}}{\Delta t} = \sigma_{ph}\left(N_{ph} - n_{hp}\Big|_i^{k+1}\right) j_h^T\Big|_i^{k+1} - \sigma_{ae}.\, n_{hp}\Big|_i^{k+1}.\, j_e^T\Big|_i^{k+1}. \tag{52}$$

which has a unique solution given by

$$n_{hp}\Big|_i^{k+1} = \frac{n_{hp}\Big|_i^{k} + \Delta t.\sigma_{ph}.N_{ph}.\, j_h^T\Big|_i^{k+1}}{1 + \Delta t.\sigma_{ph}\, j_h^T\Big|_i^{k+1} + \Delta t.\sigma_{ae}\, j_e^T\Big|_i^{k+1}} \tag{53}$$

for which the discrete maximum principle holds

$$0 \leq n_{hp}\Big|_i^{k} \leq N_{ph}. \tag{54}$$

Moreover thanks to the fixed point technique, we have the following nonlinear iteration

$$n_{hp}\Big|_i^{k+1,p+1} = \frac{n_{hp}\Big|_i^{k} + \Delta t.\sigma_{ph}.N_{ph}.\, j_h^T\Big|_i^{k+1,p}}{1 + \Delta t.\sigma_{ph}\, j_h^T\Big|_i^{k+1,p} + \Delta t.\sigma_{ae}\, j_e^T\Big|_i^{k+1,p}} \tag{55}$$

Let us construct the finite volume discretization. We integrate Eq.(**??**) over control volume $\Omega_i \times [t_k, t_{k+1}]$ to obtain

$$\begin{aligned} &\int_{\Omega_i} \left(n_{hp}(z,t^{k+1}) - n_{hp}(z,t^k)\right) dz \\ = \;& \int_{t^k}^{t^{k+1}} \left(\int_{\Omega_i} \sigma_{ph}\left(N_{ph} - n_{hp}(z,t)\right).j_h^T(z,t) - \sigma_{ae}.n_{hp}(z,t).j_e^T(z,t)\right) dt \end{aligned} \tag{56}$$

A cell-centered approximation is used for n_{hp}, then

$$\int_{\Omega_i} \left(n_{hp}(z)^{k+1} - n_{hp}(z)^k\right) dz = h_i \left(n_{hp}\Big|_i^{k+1} - n_{hp}\Big|_i^{k}\right). \tag{57}$$

But a vertex-centered approximation is used for $j_{e\pm,h\pm}(z,t)$, so we apply a first order approximation to the integral, i.e. we evaluate the integrand,which is a fonction of $j_{e\pm,h\pm}(z,t)$ at $z = z_i$ while $n_{hp}(z,t)$ is a constant over $\Omega_i \times [t^k, t^{k+1}]$ and equal to $n_{hp}\Big|_i^{k+1}$, to obtain

$$\begin{aligned} &\int_{t^k}^{t^{k+1}} \left(\int_{\Omega_i} \sigma_{ph}\left(N_{ph} - n_{hp}(z,t)\right).j_h^T(z,t) - \sigma_{ae}.n_{hp}(z,t).j_e^T(z,t)\right) dt \\ = \;& h_i \Delta t \left(\sigma_{ph}\left(N_{ph} - n_{hp}\Big|_i^{k+1}\right) j_h^T\Big|_i^{k+1} - \sigma_{ae}.\, n_{hp}\Big|_i^{k+1}.\, j_e^T\Big|_i^{k+1}\right). \end{aligned} \tag{58}$$

We now prove by induction that the discrete maximum principle holds.

– For $k = 0$, thanks to the initial condition, we have $\forall i \in [1, I],\ n_{hp}\Big|_i^0 = 0 \in \Big[0, N_{ph}\Big]$, so the condition is fulfilled.

– For a given time index k, let us assume that $n_{hp}\Big|_i^k \in \Big[0, N_{ph}\Big]$. Computation of $n_{hp}\Big|_i^{k+1}$ is given by expression

$$n_{hp}\Big|_i^{k+1} = \frac{n_{hp}\Big|_i^k + \Delta t.\sigma_{ph}\ N_{ph}.\ j_h^T\Big|_i^{k+1}}{1 + \Delta t.\sigma_{ph}.\ j_h^T\Big|_i^{k+1} + \Delta t.\sigma_{ae}.\ j_e^T\Big|_i^{k+1}} = \alpha.\ n_{hp}\Big|_i^k + \beta.N_{ph} \tag{59}$$

where

$$\left(1 + \Delta t.\sigma_{ph}.\ j_h^T\Big|_i^{k+1} + \Delta t.\sigma_{ae}.\ j_e^T\Big|_i^{k+1}\right)\alpha = 1, \tag{60}$$

$$\left(1 + \Delta t.\sigma_{ph}.\ j_h^T\Big|_i^{k+1} + \Delta t.\sigma_{ae}.\ j_e^T\Big|_i^{k+1}\right)\beta = \Delta t.\sigma_{ph}.\ j_h^T\Big|_i^{k+1}. \tag{61}$$

but $\alpha \geq 0,\ \beta \geq 0,\ \alpha + \beta \leq 1$, hence $0 \leq n_{hp}\Big|_i^{k+1} \leq \max\left(n_{hp}\Big|_i^k, N_{ph}\right) = N_{ph}$. So the discrete maximum principle is verified for $n_{hp}\Big|_i^{k+1}$.

A similar result can be stated and proved for the discrete approximation of trapped electron's equation.

4.3 Numerical simulations

4.3.1 Analysis of the influence of E_{kin}

In this subsection we investigate the sensibility of $Q_p(t)$ and $ees(t)$ with respect to the energy of the primary electrons. We assume that N_{pe}, N_{ph} and cross sections $\sigma_{ae,h}$ are fixed.

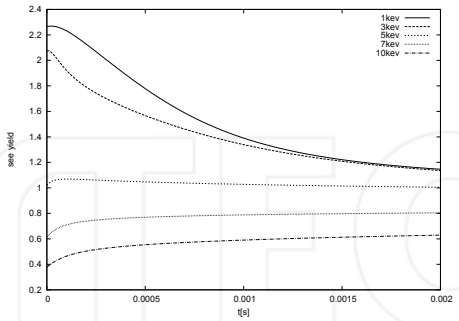

Fig. 6. Evolution of the secondary electron emission ratio as a function of time t, for various values of E_{kin}.

The behaviour of *see* with respect to E_{kin} is presented in Fig.6 and shows that for small values of E_{kin} the ratio starts from a value greater than one and decreases down to one very quickly. On the other hand for values of E_{kin} greater than 5 kev, the ratio starts below one, and strictly increases to the asymptotic value of one.

Spatial profiles of electron current $j_{e-,+}(z,t)$ and holes currents $j_{h-,+}(z,t)$ are similar in shape and amplitude, hence we only repesented in Fig.7. j_{e-} profiles. It is worth mentioning that

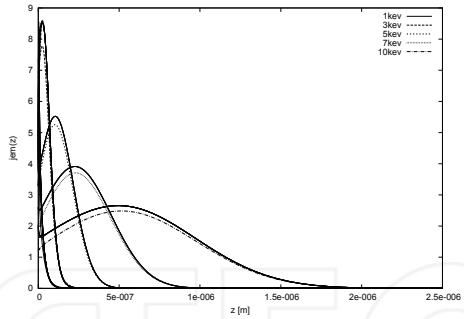

Fig. 7. Spatial distribution of electron current $j_{e-}(z,t)$ over domain $[0,L]$, for various values of E_{kin} at times $k \times 200.10^{-6}$, with $0 \leq k \leq 10$.

increasing E_{kin} induces that the maximum of $j_c(z,t)$ decreases and the profiles are diffused pushed towards $z = L$. This result is correlated with the shape of the source term $S_e(z)$ which varies accordingly when E_{kin} increases.
Trapped holes $n_{hp}(z,t)$ and trapped electrons $n_{ep}(z,t)$ are respectively represented in Fig.9 and Fig.8. The maximum of $n_{ep}(z,t)$ is smaller than the maximum of $n_{hp}(z,t)$ for each value of E_{kin} and always decreases when E_{kin} increases while the spatial profiles are smeared out.
The variation of $\log(ees(Qp))$ is represented in Fig.10 and shows a significant difference depending on the value of E_{kin}. When E_{kin} is below 5 kev, a strictly superlinear smooth decreasing profile is observed. On the other hand when E_{kin} is higher than 5 kev, the profiles have a high curvature.
Fig.11 is an enlarged representation of electric field $E(z,t)$. Three different domains can be observed for each value of E_{kin} and for each time step. A) a thin boundary layer located near the interface $z = 0$ where the $E(z,t)$ is stiff, B) a central part where $E(z,t)$ is oscillating and a third part near the interface $z = L$ where $E(z,t)$ is flat.

4.3.2 Analysis of the influence of the value of N_{pe} and N_{ph}

In this subsection we assume that the kinetic energy of the incident electron beam is constant and given the value of 4 kev, and study the influence of N_{pe}, and N_{ph} on the variation of $sse(t)$ and $Q_p(t)$. The trend observed in the numerical simulations appears independent of E_{kin}.

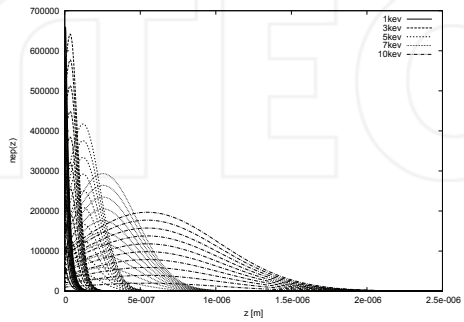

Fig. 8. Spatial distribution of trapped electrons $n_{ep}(z,t)$ over domain $[0,L]$, for various values of E_{kin} at times $k \times 200.10^{-6}$, with $0 \leq k \leq 10$.

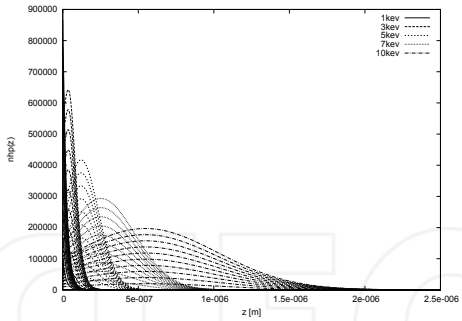

Fig. 9. Spatial distribution of trapped holes $n_{hp}(z,t)$ over domain $[0,L]$, for various values of E_{kin} at times $k \times 200.10^{-6}$, with $0 \leq k \leq 10$.

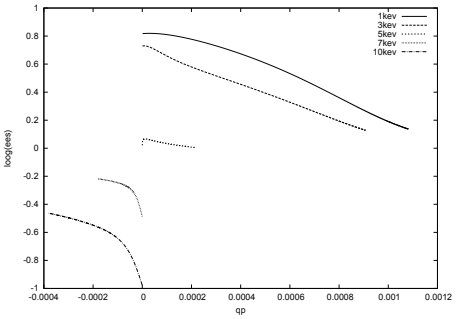

Fig. 10. Evolution of $\log(ees)$ as function Q_p for various values of E_{kin}.

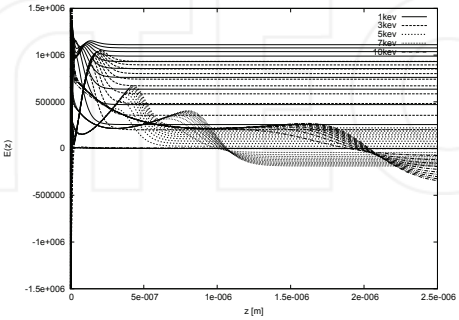

Fig. 11. Spatial distribution of electric field $E(z,t)$ over domain $[0,L]$, for various values of E_{kin} at times $k \times 200.10^{-6}$, with $0 \leq k \leq 10$.

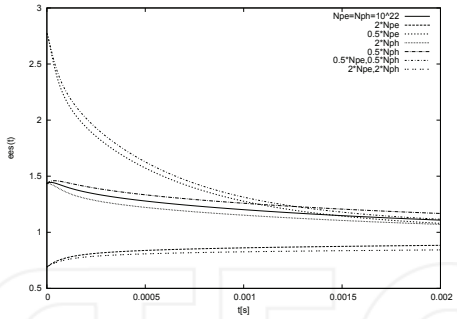

Fig. 12. Sensibility of the temporal evolution of see(t) when both values of N_{pe} and N_{ph} are varied simultaneously or independently for E=4keV.

As seen on Fig.12, reducing in/dependently N_{pe} and N_{ph} leads to a significant increase of the secondary electron emission ratio well above 1. On the other hand reducing in/dependently N_{pe} and N_{ph} leads to a significant decrease of the total trapped charge $Q_p(t)$.
The analysis of the evolution of $\log(ees(Q_p(t)))$ represented in Fig.13 shows that setting N_{pe} and varying N_{ph} induces that the curves are parallel, but converging to the same point where $Q_p = 0$. On the other hand, setting N_{ph} and varying N_{pe} above or below the initial value of N_{pe} leads to a much wider variation of *see* above or below 1 as seen on Fig.12.
As a conclusion, the most important parameter in these simulations appears to be N_{pe}.

4.3.3 Comparison between numerical computations and experimental results

Preliminary promising results are presented in Fig.14.

5. Transient see computation by a reaction-diffusion method

In section 5, we extend the reformulation of the two-fluxes modelling presented in section 4 into a reaction-diffusion modelling. The main strength of this new approach is the ability to be extended in two/three spatial dimensions. Moreover, it is more difficult to extend in two/three-spatial dimensions the two-fluxes approach borrowed from the radiative transfer (Chandrasekhar 1961), hence this new approach seems more promising.

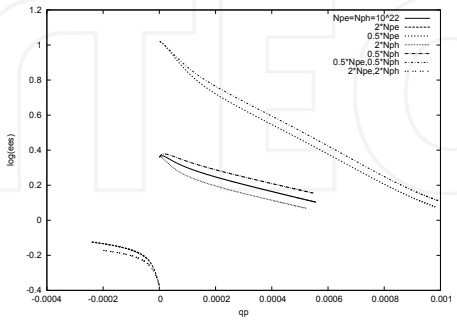

Fig. 13. Evolution of $\log(ees)$ as function Q_p when both values of N_{pe} and N_{ph} are varied simultaneously or independently for E=4keV.

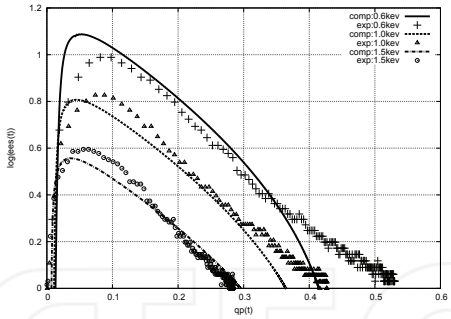

Fig. 14. Comparison between experimental and computed values of secondary electron emission yield $see(t)$ versus trapped charge $Q_p(t)$.

5.1 Mathematical Modelling

We present the modelling composed of a set of two, one dimensional reaction-diffusion equations for electrons/holes coupled with Gauss equation for the electric field and an equation for trapped electrons/holes evolution.

5.1.1 Governing equation for the electric field $E(z,t)$

The local conservation equation for the electric field $E(z,t)$ writes

$$\nabla.E\left(z,t\right)=\frac{\rho\left(z,t\right)}{\varepsilon_0\varepsilon_r} \tag{62}$$

The boundary condition at $z=0$, derived from an electrostatic analysis is written

$$E\left(0,t\right)=-\frac{1}{\varepsilon_0\varepsilon_r\left(1+\varepsilon_r\right)}\int_0^L\rho\left(z,t\right)dz \tag{63}$$

5.1.2 Governing equation for charge density $\rho(z,t)$

We define the overall current flux $j_T\left(z,t\right)=j_e\left(z,t\right)-j_h\left(z,t\right)-j_0\,j_{prim}\left(z\right)$. The conservation law expressing the evolution of charge density $\rho(z,t)$ is written

$$\frac{\partial\rho\left(z,t\right)}{\partial t}+\nabla.j_T\left(z,t\right)=0 \tag{64}$$

with initial condition $\rho\left(z,0\right)=0$ expressing the lack of charge.

5.1.3 Governing equations for the number of free charges $\left(n_c\left(z,t\right)\right)_{c\in C}$ and current fluxes $j_c(z,t)$

For charge c, the number of trapped charge, either electrons or holes, $n_c\left(z,t\right)$ is based on the following balance equation

$$\frac{\partial n_c}{\partial t}\left(z,t\right)+\nabla.j_c\left(z,t\right)=2S_c\left(z\right)-\left(\sigma_c^{abs}v\right)n_c\left(z,t\right) \tag{65}$$

The current flux for charge c $j_c\left(z,t\right)$ is related to the number of free charges $n_c\left(z,t\right)$ thanks to the equation

$$j_c\left(z,t\right)=-D_c\nabla n_c\left(z,t\right)+n_c\left(z,t\right)\,\mu_c s_c E\left(z,t\right). \tag{66}$$

For a given charge $c \in C$, its sign s_c is set to be $+1$ for the holes and -1 for the electrons and its mobility is represented by $\mu_c \geq 0$. The diffusion coefficient D_c is defined by $D_c = \frac{v_c}{\sigma_c^{trans}}$, where $\sigma_c^{trans} = \sigma_c^{abs} + 2\sigma_c^{diff}$. Hence the partial differential equation related to the evolution of $n_c(z,t)$ is rewritten

$$\frac{\partial n_c}{\partial t}(z,t) + \nabla.(-D_c \nabla n_c(z,t) + n_c(z,t)\ \mu_c s_c E(z,t)) = 2S_c(z) - \left(\sigma_c^{abs} v\right) n_c(z,t) \tag{67}$$

It is a linear reaction-convection-diffusion equation of parabolic type for unknown $n_c(z,t)$, expressed in conservation form. Two boundary conditions at interfaces $z = 0$ and $z = L$ must be given in order for the problem to be well-posed. Following the discussion presented in Section 3, we use the following conditions that depend on the charge c.

– at $z = 0$

$$\begin{aligned} -D_e \frac{\partial n_e(z,t)}{\partial z} - \mu_e n_e(z,t) E(z,t)\Big|_{z=0} &= -\frac{\kappa}{2-\kappa} v_e n_e(0,t), \\ -D_h \frac{\partial n_h(z,t)}{\partial z} + \mu_h n_h(z,t) E(z,t)\Big|_{z=0} &= 0. \end{aligned}$$

– at $z = L$

$$\begin{aligned} -D_e \frac{\partial n_e(z,t)}{\partial z} - \mu_e n_e(z,t) E(z,t)\Big|_{z=L} &= v_e n_e(L,t), \\ -D_h \frac{\partial n_h(z,t)}{\partial z} + \mu_h n_h(z,t) E(z,t)\Big|_{z=L} &= v_h n_h(L,t) \end{aligned}$$

5.2 Numerical scheme

We discuss an implicit finite-volume scheme, on a non uniform spatial grid and focus the analysis on the discrete maximum principle fulfilled by the numerical scheme for this linear reaction-convection-diffusion equation. The number of free charges $n_c(z,t)$ is positive, a discretization of the equation must give positive values. We know that for convection diffusion equation, upwind schemes induce artificial numerical diffusion that can be monitored thanks to the local Peclet number. Moreover a boundary layer characterizes the modelling. A discrete maximum principle must be verified for the discretization of

$$\nabla.(n_c(z,t)\mu_c s_c E(z,t)) \tag{68}$$

To this end, the finite volume discrete approximation is given by the following expression, where to simplify the notations, we have defined $v_c(z,t) = \mu_c s_c E(z,t)$,

$$\int_{\Omega_i} \nabla.(n_c(z,t)\, v_c(z,t)) = n_{i+\frac{1}{2}}^{k+1} v_{i+\frac{1}{2}}^{k+1} - n_{i-\frac{1}{2}}^{k+1} v_{i-\frac{1}{2}}^{k+1}. \tag{69}$$

Taking into account the signs of $v_{i+\frac{1}{2}}$ leads to

– if $v_{i+\frac{1}{2}}^{k+1} \geq 0$, then $n_{i+\frac{1}{2}}^{k+1} = n_i^{k+1}$, while if $v_{i+\frac{1}{2}}^{k+1} \leq 0$, then $n_{i+\frac{1}{2}}^{k+1} = n_{i+1}^{k+1}$.

A discrete maximum principle is then easily established following the method described in section 3. Work is in progress to analyse the numerical results.

6. Numerical software sirena

We describe briefly the architecture of our numerical software sirena. It is a toolbox for the numerical solution either by a two-fluxes method or by a reaction-diffusion method of the *see* yield. It is written in C language and consists of distinct modules that compute, the initial mesh either uniform or geometrically refined near $z = 0$, and solve the electric field equation, trapped charge density equation, etc . Several specialized data structures are used. The visualization is possible thanks to scripts written for gnuplot software but also in VTK format for the animated visualization of time-dependent quantities. It has been compiled under windows xp with a free C compiler, DEV-CPP while under linux with gnu gcc. A typical run with an adequate refined mesh requires less than a minute on a standard laptop.

7. Conclusions and perspectives

In this book chapter, we have presented a modelling for the computation of the initial and transient true see yield following a *traditional* two-fluxes approach. We have stressed the discrete maximum principle property of the conservative finite-volume numerical discretization presented in this chapter. A new asymptotic expression for the initial true see yield was presented and discussed.
A new approach, in this field, based on a reaction-diffusion modelling was presented for both initial and transient computation of true see yield. As in the two-fluxes approach, we have analyzed the discrete maximum principle properties of the finite-volume discretization scheme and provided some numerical simulations.
Finally, a numerical software **sirena** freely available upon request was presented.
In the future, We plan to extend this reaction-diffusion approach in two-spatial dimensions in order to perform numerical simulations of charge trapping inside the material for focalized electron beam, because in this case, lateral and longitudinal distributions of electrons/holes are important. This requires the knowledge for the creation of free electron/holes inside the sample. There appears to be no expression for such term in the litterature, which has a pear-like shape according to some monte carlo computations. We plan to use such computations and curve-fitting in order to obtain a law that will be plugged into the 2D version of **sirena**.

8. References

Aoufi, A. & Damamme, G. (2009). Numerical computation of secondary electron emission yield by a two-fluxes method, *Proceedings of ICNAAM 2009*, AIP, Rethymno - Crete.

Aoufi, A. & Damamme, G. (n.d.). 1d numerical simulation of charge trapping in an insulator submitted to an electron beam irradiation
part i: Computation of the initial secondary electron emission yield, *Applied Mathematical Modelling* . `www.elsevier.org`.

Fitting, H.-J. (1974). *Phys. Stat. Sol. A.* 26: 525–535.

G. Damamme, C. L. & Reggi, A. D. (1997). *IEEE Trans.Dielec.Elect.Insul* Vol. 5(No. 4): 558–584.

H.-J. Fitting, H. G. & Wild, W. (1977). *Physical Status Solid (a)* (43): 185–190.

I.A.Glavatskikh, V. S. K. & Fitting, H.-J. (2001). 'self-consistent electrical charging of insulating layers and metal-insulator-semiconductor structures', *J. Appl. Phys* (89): 440–448.

Levy, L. (2002). *Metal Charging*, Cepadues Edition.

Numerical Simulations - Applications, Examples and Theory
Edited by Prof. Lutz Angermann

ISBN 978-953-307-440-5
Hard cover, 520 pages
Publisher InTech
Published online 30, January, 2011
Published in print edition January, 2011

This book will interest researchers, scientists, engineers and graduate students in many disciplines, who make use of mathematical modeling and computer simulation. Although it represents only a small sample of the research activity on numerical simulations, the book will certainly serve as a valuable tool for researchers interested in getting involved in this multidisciplinary ï¬eld. It will be useful to encourage further experimental and theoretical researches in the above mentioned areas of numerical simulation.

InTech Europe
University Campus STeP Ri
Slavka Krautzeka 83/A
51000 Rijeka, Croatia
Phone: +385 (51) 770 447
Fax: +385 (51) 686 166
www.intechopen.com

InTech China
Unit 405, Office Block, Hotel Equatorial Shanghai
No.65, Yan An Road (West), Shanghai, 200040, China
中国上海市延安西路65号上海国际贵都大饭店办公楼405单元
Phone: +86-21-62489820
Fax: +86-21-62489821